Detection of radio-frequency magnetic fields using nonlinear magneto-optical rotation

M. P. Ledbetter,* V. M. Acosta, S. M. Rochester, and D. Budker†
Department of Physics, University of California at Berkeley, Berkeley, California 94720-7300, USA

S. Pustelny
Centrum Badań Magnetooptycznych, Instytut Fizyki im. M. Smoluchowskiego, Uniwersytet Jagielloński, Reymonta 4, 30-059 Kraków, Poland

V. V. Yashchuk
Advanced Light Source Division, Lawrence Berkeley National Laboratory, Berkeley, California 94720, USA
(Received 21 September 2006; revised manuscript received 4 December 2006; published 8 February 2007)

We describe a room-temperature alkali-metal atomic magnetometer for detection of small, high-frequency magnetic fields. The magnetometer operates by detecting optical rotation due to the precession of an aligned ground state in the presence of a small oscillating magnetic field. The resonance frequency of the magnetometer can be adjusted to any desired value by tuning the bias magnetic field. Based on experimentally measured signal-to-noise ratio, we demonstrate a sensitivity of 100 pG/$\sqrt{\text{Hz}}$ (rms) in a 3.5-cm-diameter paraffin coated cell. Assuming detection at the photon shot-noise limit, we project a sensitivity as low as 25 pG/$\sqrt{\text{Hz}}$ (rms).

DOI: 10.1103/PhysRevA.75.023405 PACS number(s): 32.80.Bx, 07.55.Ge, 42.65.−k

I. INTRODUCTION

Detection of small, rapidly oscillating magnetic fields is the cornerstone of experimental techniques such as nuclear magnetic resonance (NMR), magnetic resonance imaging (MRI), nuclear quadrupole resonance (NQR) [1] and has been used in tests of physics beyond the standard model [2]. Most atomic magnetometers (for example, see Refs. [3–6]) are designed to detect slowly varying magnetic fields and hence are not ideally suited for the aforementioned applications. In recent work, Savukov *et al.* [7] demonstrated a tunable, radio-frequency (rf) alkali vapor magnetometer, achieving a sensitivity of 20 pG/$\sqrt{\text{Hz}}$, with the sensor operating at 190 °C.

Here we discuss an atomic magnetometer sensitive to high-frequency magnetic fields based on nonlinear magneto-optical rotation (NMOR). In this scheme optical rotation arises due to the response of an aligned atomic ground state to a small oscillating magnetic field near the Zeeman resonance frequency which can be adjusted to any desired value by tuning the bias magnetic field. Based on experimentally observed signal-to-noise ratio, we demonstrate a sensitivity of 100 pG/$\sqrt{\text{Hz}}$ (rms) at 7 kHz within a bandwidth of about 50–100 Hz depending on light power. Based on the resonance amplitude and photon shot-noise limited polarimetry, we project a sensitivity of about 25 pG/$\sqrt{\text{Hz}}$ (rms).

Despite somewhat lower sensitivity than reported in Ref. [7], for many applications, the magnetometer described here has the significant advantage that the sensor operates much closer to room temperature (the highest temperature used in this work was 48 °C). Additionally, using an aligned state rather than an oriented state produces smaller external magnetic fields which can have a back reaction on the sample of interest. Furthermore, the optical pumping and probing scheme uses only a single, low power laser beam ($\lesssim$100 μW), facilitating the use of microfabrication techniques, promising for the development of compact portable atomic magnetometers [8].

Such a magnetometer may find application in NQR [7] where the signal occurs at a fixed resonance frequency or in NMR spectroscopy where high spectral resolution is required to observe small splittings of NMR lines, due to, for example, scalar spin-spin (J) coupling between nuclei of the form $J\mathbf{I}_1\cdot\mathbf{I}_2$. Such couplings can yield valuable information on molecular structure [9,10] and can be difficult to access in high-field environments where inhomogeneities in the applied field or differences in diamagnetic susceptibility limit the spectral resolution. Hence recent attention has been given to performing such measurements in a low-field environment using broadband, low transition-temperature superconducting quantum interference devices (SQUIDs) [9] or inductive detection [10]. As inductive detection becomes less efficient at low frequencies, the technique described in this paper offers the possibility of significant gains in signal-to-noise ratio without requiring cryogenics.

II. RADIO-FREQUENCY NMOR RESONACE

An alkali-metal vapor (here we work with ^{87}Rb, with nuclear spin $I=3/2$) contained in a glass cell with antirelaxation coated walls is placed in a z directed bias field $\mathbf{B}_0=B_0\hat{\mathbf{z}}$, corresponding to Larmor frequency $\Omega_L=g\mu_B B_0$, where μ_B is the Bohr magneton and $g\approx 2/(2I+1)$ is the Landé factor ($\hbar=1$). Linearly polarized light propagating in the x direction with polarization in the z direction, tuned to the $D1$ ($F=2\rightarrow F'=1$) transition, passes through the cell, optically pumping an aligned state, as illustrated in Fig. 1. We apply a small oscillating magnetic field transverse to the

*Electronic address: ledbetter@berkeley.edu
†Electronic address: budker@berkeley.edu

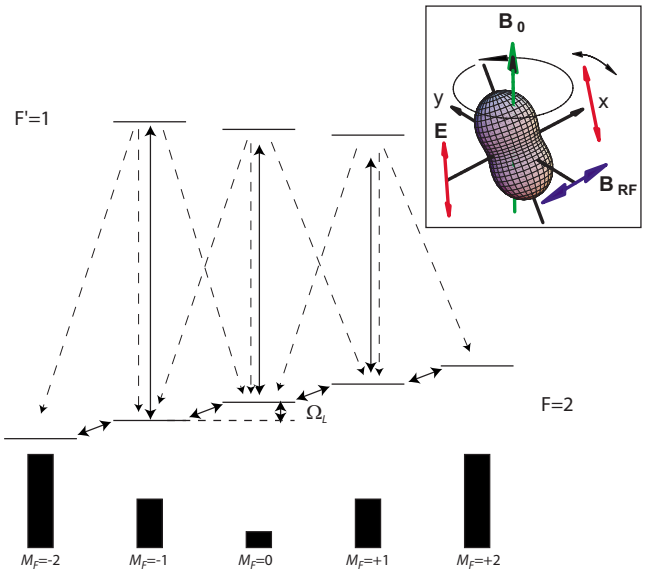

FIG. 1. (Color online) Linearly polarized light, resonant with the $D1$ $(F=2\rightarrow F'=1)$ transition, with polarization vector along $\mathbf{B}_0$, produces an aligned ground state via optical pumping. Double headed vertical arrows indicate laser induced transitions between ground and excited states; dashed lines indicate transitions due to spontaneous decay. Ground-state populations, indicated by the solid black bars, are schematic only. A small rf magnetic field oscillating close to Ω_L, transverse to $\mathbf{B}_0$, establishes coherences between neighboring M_F states. Inset: surface whose radius represents the probability for finding maximal projection of ground-state angular momentum along a given direction (see, for example, Ref. [12]).

bias field, $B_x=B_1\cos\omega_{rf}t$, and work in the regime where $g\mu_B B_1 \ll \gamma_{rel}$ (γ_{rel} is the relaxation rate of ground-state polarization) so that the oscillating magnetic field induces only ground-state transitions with $|\Delta M_F|=1$.

We begin by assuming the light power is weak enough so that the saturation parameter relating the optical excitation rate to the ground-state relaxation rate [11]

$$\kappa = \frac{d^2E^2}{\hbar^2\Gamma_D\gamma_{rel}}\frac{V_{beam}}{V_{cell}} \tag{1}$$

is small compared to unity. In Eq. (1), d is the electric dipole matrix element of the optical transition, E is the light electric field, Γ_D is the Doppler broadened width of the optical transition, V_{cell} is the volume of the cell, and V_{beam} is the volume contained within the intersection of beam and cell. When $\kappa \ll 1$ only the rank 2 (quadrupole) polarization moment is pumped by linearly polarized light.

The oscillating rf magnetic field can be resolved into components co- and counter-rotating (parallel or antiparallel to the direction of Larmor precession, respectively), each of magnitude $B_1/2$. Transforming to the co-rotating frame the counter-rotating component rapidly averages to zero [13] and the magnetic field is

$$\mathbf{B}' = \frac{\Omega_L - \omega_{rf}}{g\mu_B}\hat{\mathbf{z}} + \frac{B_1}{2}\hat{\mathbf{x}}. \tag{2}$$

In steady state, an equilibrium is reached between optical pumping of alignment along the z axis, precession around $\mathbf{B}'$ and relaxation, resulting in an aligned state tilted away from the z axis, as shown inset in Fig. 1. When $\omega_{rf}=\Omega_L$, the z component in Eq. (2) vanishes resulting in the maximum angle between the aligned state and the z axis. When we transform back into the lab frame, the tilted alignment precesses about the z axis. The tilted alignment generates optical rotation through linear dichroism (see, for example, Ref. [14]), maximal when the alignment is in the yz plane and none when it is in the xz plane, resulting in polarization rotation of the light beam that is modulated at ω_{rf}. For sufficiently small values of B_1 $(g\mu_B B_1 \ll \gamma_{rel})$, the amplitude of the polarization rotation is linear in B_1. For the measurements presented here $g\mu_B B_1=0.48\ \mathrm{s}^{-1}$ and the zero light power relaxation rate was $\gamma_{rel}=60\ \mathrm{s}^{-1}$. We verified experimentally that the amplitude of optical rotation was linear in B_1 in this regime. For larger values of B_1, rapid precession about B_1 near resonance can wash out the alignment induced by optical pumping, leading to nonlinear behavior in B_1, similar to that observed in Ref. [15].

The description becomes slightly more complicated for higher light power and for light frequency detuned from optical resonance. Under these conditions, ac Stark shifts lead to differential shifts of the ground-state energy levels. In conjunction with precession in the rf magnetic field, this results in alignment-to-orientation conversion (AOC) (see Ref. [16] and references therein) in the rotating frame and a splitting of the rf NMOR resonance as discussed briefly below. Doppler broadening can also lead to AOC effects, even for resonant light [16]. An additional high-light-power effect is the generation of the hexadecapole (rank 4) polarization moment [17,18]. We find experimentally that optimal sensitivity is achieved when the saturation parameter is close to unity, but density-matrix calculations indicate that the hexadecapole contribution to the ground-state polarization is small compared to that of the quadrupole contribution for these conditions.

III. EXPERIMENTAL SETUP

A schematic of the experimental setup is shown in Fig. 2. The measurements reported in this work were performed with an evacuated, paraffin-coated spherical cell (3.5-cm diameter) containing isotopically enriched ^{87}Rb (nuclear spin $I=3/2$). The paraffin coating enables atomic ground-state polarization to survive several thousand wall collisions [19–21]. The cell is placed inside a double-wall oven, temperature-controlled by flowing warm air through the space between the walls so that the optical path is unperturbed. A set of four nested μ-metal layers provides a magnetically shielded environment, with a shielding factor of approximately 10^6 [22]. Inside the innermost shield (cubic in profile) is a set of square, solenoidal coils. The coils are arranged so that each generates a magnetic field normal to a different set of parallel faces of the inner shield, yielding control of all three components of the magnetic field. The combination of currents applied to the coils and the image currents in the magnetic shields create "infinitely" long solenoids in three different directions. The atoms traverse the cell many times during the course of one relaxation period, ef-

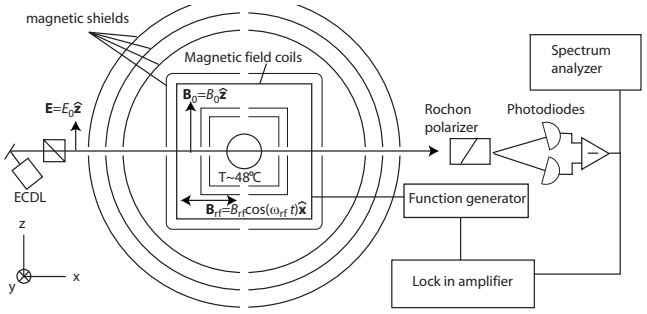

FIG. 2. Schematic of the experimental setup. An evacuated, paraffin coated cell is placed inside a double-wall oven. Temperature is controlled by flowing warm air through the space between the oven walls. A set of μ-metal layers provides a magnetically shielded environment, and a set of coils maintains a stable, homogeneous magnetic field in the z direction. An additional coil generates a small oscillating magnetic field in the x direction. Linearly polarized light from an external-cavity diode laser passes through the cell and a balanced polarimeter monitors the polarization of the light as it exits the cell.

fectively averaging the magnetic field over the cell, leaving our measurements insensitive to field gradients [23]. We apply a static magnetic field B_0 in the z direction and a small oscillating magnetic field $B_1\cos(\omega_{rf}t)$ in the x direction (unless stated otherwise, $B_1=110$ nG and $B_0\approx 10$ mG). Eddy currents in the inner shield layer could alter the amplitude of the oscillating field as a function of ω_{rf}. Using a pickup coil, we checked that the amplitude of the oscillating magnetic field varied by less than 10% from 100 Hz to 10 kHz at the location of the cell.

A collimated beam with diameter ≈ 3 mm from an external-cavity diode laser, propagates in the x direction with polarization vector in the z direction. Unless stated otherwise, these measurements were performed with the light tuned to the center of the $F=2\rightarrow F'=1$ transition (henceforth referred to as optical resonance). On account of distortion of the light beam by the cell, we were able to collect only 20% of the light that passed through the cell (determined by tuning the laser far away from optical resonance). The polarization of this light was monitored using a balanced polarimeter incorporating a Rochon polarizer, two photodiodes, and a differential amplifier, and detected synchronously using a lock-in amplifier. Number density was determined by monitoring the transmission of a low-power beam through the cell as a function of laser frequency. For the measurements reported here, the cell temperature was 48 °C, and the measured number density was $n=7\times 10^{10}$ (within 20% of that expected from the saturated vapor pressure at this temperature), corresponding to approximately one absorption length for resonant light.

IV. rf MAGNETOMETER PERFORMANCE

In Fig. 3 we plot the noise spectrum for the current experimental setup as measured by an SRS770 spectrum analyzer at the output of the balanced polarimeter. Optimization of parameters is discussed in the next two sections. The large

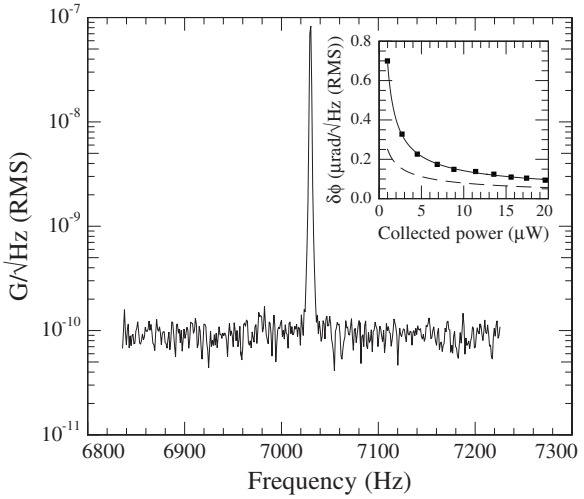

FIG. 3. rf magnetic noise spectrum. The large peak is an applied field of 83 nG (rms) at Ω_L. Light power into the cell was 40 μW. Shown inset is the polarimeter noise (squares) as a function of total power collected by the polarimeter. The solid line is a fit based on Eq. (3) and the dashed line represents photon shot noise.

peak is an applied field of 83 nG (rms) to calibrate the magnetometer. Baseline noise is about 100 pG/$\sqrt{\text{Hz}}$ (rms). In order to assess the performance of the polarimeter, shown inset in Fig. 3 is the measured noise floor (squares) as a function of light power incident on the polarimeter. The dashed line represents photon shot noise $\delta\phi_{ph}=1/(2\sqrt{\Phi_{ph}})=0.35$ μrad$\sqrt{\mu\text{W}}/\sqrt{\text{Hz}}$ (rms) where Φ_{ph} is the number of photons per second incident on the polarimeter [24]. For light power greater than about 10 μW, the measured noise is within 20% of the photon shot-noise limit. Polarimeter noise can be parametrized by

$$\delta\phi=\sqrt{\zeta_{ph}^2/P+\zeta_{amp}^2/P^2}. \tag{3}$$

Here P is the power incident on the polarimeter and ζ_{ph} and ζ_{amp} parametrize photon shot noise and the differential amplifier noise, respectively. The solid line overlaying the data is a fit based on Eq. (3), resulting in $\zeta_{amp}=0.55$ μrad $\mu\text{W}/\sqrt{\text{Hz}}$ (rms) and $\zeta_{ph}=0.41$ μrad$\sqrt{\mu\text{W}/\text{Hz}}$ (rms), close to the theoretically predicted value. Hence amplifier noise is the dominant contribution for incident light power less than about 2 μW and photon shot noise dominates for higher light power.

V. EXPERIMENTAL ANALYSIS OF rf NMOR RESONANCE

In Fig. 4(a) we plot the in-phase component of the synchronously detected optical rotation as a function of light frequency for $\omega_{rf}=\Omega_L$. For these data, the light power was 60 μW (850 $\mu\text{W}/\text{cm}^2$). In Fig. 4(b) we plot the partially saturated transmission curve under the same experimental conditions. The background slope of the transmission curve is due to varying laser intensity as the diode laser feedback grating is swept. The largest optical rotation occurs for light tuned near the center of the $F=2\rightarrow F'=1$ transition, similar

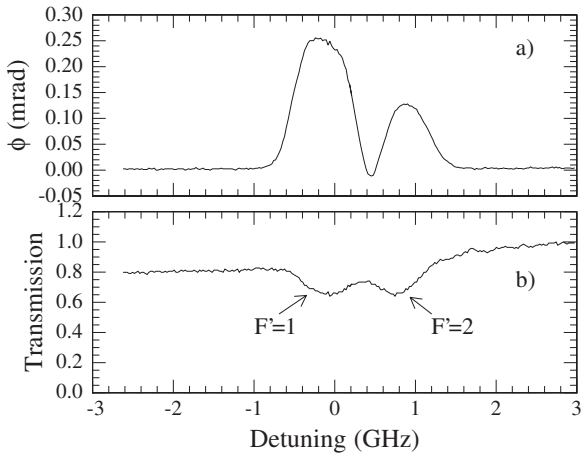

FIG. 4. (a) Synchronously detected optical rotation and (b) transmission spectra as a function of light frequency for a light power of 60 μW and $\omega_{rf}=\Omega_L$. The overall slope on the transmission curve is due to the change in incident laser power.

to observations of nonlinear Faraday rotation induced by a static magnetic field [25]. At the light powers for which we obtained optimal sensitivity on the $F=2$ component, optical rotation on the $F=1$ component was at least an order of magnitude smaller than that produced by the $F=2$ component.

In the main panel of Fig. 5 we show the synchronously detected in-phase (stars) and quadrature (squares) compo-

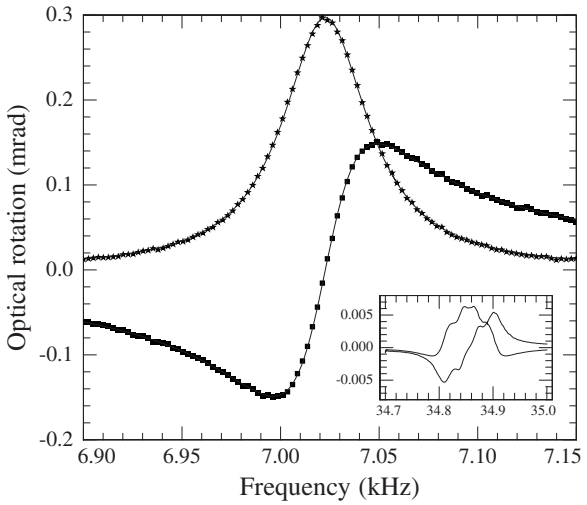

FIG. 5. In-phase (stars) and quadrature (squares), synchronously detected optical-rotation signal as a function of the frequency of the applied oscillating magnetic field. Overlaying the data (solid lines) are fits to a single dispersive or absorptive Lorentzian. For these data, the light was tuned approximately to the center of the $F=2\rightarrow F'=1$ transition and the power was 40 μW. Inset: Optical-rotation signals for light detuned approximately one Doppler-broadened linewidth (≈300 MHz) towards lower frequencies from the $F=2\rightarrow F'=1$ transition. Light power was 360 μW, and the cell temperature was 20 °C. ac Stark shifts result in a splitting of the resonance. Units are the same as in the main panel. The overall position of the resonance is different from that in the main panel because the bias field differed by a factor of 5.

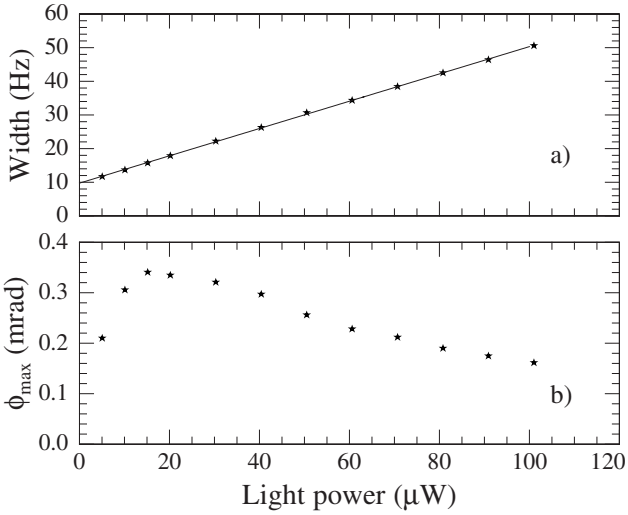

FIG. 6. (a) Half width at half maximum of the in-phase component of the rf NMOR resonance shown in Fig. 5 as a function of light power. The solid line overlaying the data is a linear fit. (b) The amplitude of the rf NMOR resonance ϕ_{max}, defined as the maximum value of the in-phase component.

nents of optical rotation for light tuned to optical resonance and incident light power of 40 μW. Overlaying the in-phase (quadrature) component is a fit to a single absorptive (dispersive) Lorentzian. As mentioned previously, under conditions of high light power and detuning far from optical resonance, differential ac Stark shifts can lead to a modification of the quantum beat frequency for different $\Delta M_F=1$ transitions resulting in a splitting of the resonance, as shown inset in Fig. 5. The overall shift of the resonance compared to that shown in the main panel is because the bias magnetic field differed by a factor of 5. The amplitude of the resonance is significantly smaller than that shown in the main panel because of the large optical detuning and due to power broadening. ac Stark shifts were discussed in some detail in Ref. [5] in the context of NMOR with frequency-modulated light. It was found that magnetometric sensitivity was reduced when the resonance was split and hence we do not focus on this behavior any further. However, we point out that ac Stark shifts may provide some degree of optical tunability of the Zeeman resonance and we will explore this possibility in future work.

In Fig. 6(a) we plot $\Delta\nu$, the half width at half maximum, of the in-phase component of the rf NMOR resonance, as a function of light power (the distance from the center of the resonance to the extrema of the quadrature signal is also given by $\Delta\nu$). Overlaying the data is a linear fit with zero-power width $\Delta\nu_0=9.7$ Hz. The intrinsic polarization relaxation rate γ_{rel} is related to $\Delta\nu_0$ via $\gamma_{rel}=2\pi\Delta\nu_0$ [26]. Ground-state relaxation in paraffin coated cells is typically dominated by electron randomization during collisions with the cell walls and through alkali-alkali spin exchange collisions (see, for example, Refs. [27,28] and references therein). The relaxation rate for the latter process is given by [29]

$$\gamma_{SE}\approx\frac{1}{2}\sigma_{SE}v_{rel}n=2\pi\times 6\times 10^{-11}\mathrm{cm}^3\mathrm{Hz}\times n. \quad (4)$$

Here $\sigma_{SE}\approx 2\times 10^{-14}$ cm^2 is the spin-exchange cross section, and $v_{rel}=\sqrt{8kT/\pi\mu}$ is the average relative speed of the at-

oms, μ is the reduced mass. The factor of 1/2 in Eq. (4) represents the approximate nuclear "slowing down" factor appropriate for a spin 3/2 nucleus (see Ref. [29] for more general formulas for different I). For a density $n=7\times10^{10}$ cm^{-3}, Eq. (4) gives $\gamma_{SE}=2\pi\times4.2$ Hz, roughly a factor of 2 smaller than the experimentally measured relaxation rate. We attribute the excess relaxation to collisions with the walls.

In Fig. 6(b) we plot the amplitude ϕ_{max} of the rf NMOR resonance shown in Fig. 5 (defined as the maximum of the in-phase component) as a function of light power. The amplitude increases as a function of light power for low light power, until reaching a maximum at around 15 μW corresponding to $\kappa\approx1.5$. Beyond saturation the amplitude decreases due to light broadening.

A complete theoretical treatment of NMOR is difficult because of the presence of hyperfine structure, Doppler broadening, velocity mixing, and evolution in the dark. Following the method outlined in Ref. [11] we performed a simplified steady-state density matrix calculation on an $F=2\rightarrow F'=1$ transition which neglects these issues, but qualitatively reproduces the salient features of our experimental data. The Hamiltonian is written in the rotating-wave approximation, neglecting terms counter rotating at either the optical or radio frequencies. The density-matrix evolution equations are formed, including terms describing spontaneous decay of the excited state, and atoms entering and leaving the interaction region (transit relaxation), and solved numerically. For conditions of high light power and detuning far from optical resonance, the model reproduces the splitting of the rf NMOR resonance shown inset in Fig. 5. When the light is tuned to optical resonance, a single feature is observed in the rf dependence of the optical rotation. The calculated power dependence of the amplitude of the resonance is similar to the experimentally observed behavior shown in Fig. 6(b). The model indicates that for light power that maximizes optical rotation (saturation), the hexadecapole contribution to the ground-state polarization is small (roughly 10%) compared to that of the quadrupole contribution.

VI. DISCUSSION

In Fig. 7 we plot the projected sensitivity of the magnetometer (stars) $\delta B_{proj}=\delta\phi(B_1/\phi_{max})$ based on the amplitude of the rf NMOR resonance shown in Fig. 6(b) and detection of the light at the photon shot noise limit. In estimating the photon shot-noise, we measure the light power after the beam passes through the shields and multiply by a factor of 5 to account for absorption of the light by the atomic vapor as well as loss of light due to distortion of the light beam by the cell. Optimum projected sensitivity of about 25 pG/$\sqrt{\text{Hz}}$ (rms) occurs at about 40–50 μW input light power and remains roughly constant out to 100 μW. For comparison, we also plot the measured noise floor (squares), determined from spectra like that shown in Fig. 3 as a function of light power. One reason for coming short of the projected sensitivity limit is the factor of 5 loss in light power which results in a factor of $\sqrt{5}$ loss in sensitivity.

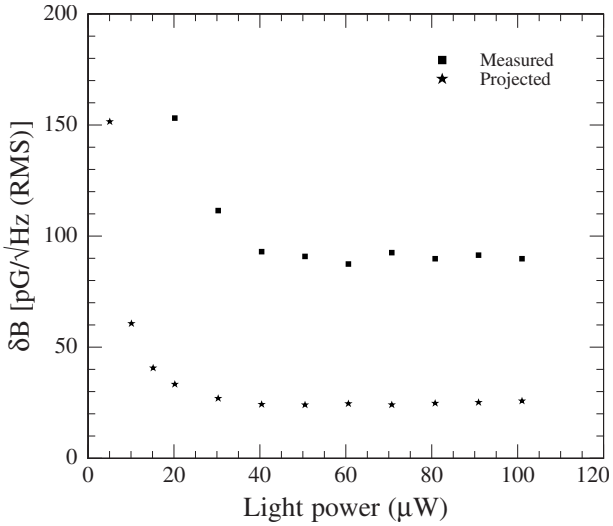

FIG. 7. Projected (stars) and experimentally measured (squares) sensitivity as a function of light power incident on the cell.

In addition to sensitivity, an important characteristic of the magnetometer is its bandwidth, defined here as full width at half maximum of the in-phase component of the rf NMOR resonance. Referring to Fig. 6, we see that the bandwidth is about 50 Hz at 40 μW. By increasing light power to 100 μW the bandwidth may be doubled with little loss in projected sensitivity.

It is interesting to compare the projected sensitivity in Fig. 7 with atomic shot noise, given by

$$\delta B_{\text{atom}}=2\frac{1}{g\mu_B}\frac{1}{\sqrt{nV_{\text{cell}}\tau}}\approx4\text{pG}/\sqrt{\text{Hz}}(\text{rms}). \tag{5}$$

Here $\tau=1/\gamma_{rel}$ is the lifetime of the ground-state polarization, and a bandwidth of 1 Hz corresponds to a measurement time of 0.5 s. The factor of 2 is due to the fact that the magnetometer is sensitive only to the co-rotating component of an oscillating magnetic field. For an optimized magnetometer, one would expect that photon shot noise (adding in quadrature to the atomic shot noise) would be comparable to the atomic shot noise [30] and hence Eq. (5) must be multiplied by a factor of $\sqrt{2}$ for a fair comparison. Thus for optimized light power, the projected sensitivity in Fig. 7 is approximately a factor of 4–5 from the limit of an ideal magnetometer. One possible explanation the projected sensitivity fails to reach the atomic shot-noise limit is the following: Atoms can be optically pumped into the $F=1$ state where they do not interact with the light, effectively decreasing the number of atoms participating in the measurement. This may be rectified by using a second laser, resonant with the $F=1$ state to "repump" atoms back into the $F=2$ state.

Finally we note that for most of the measurements presented here, the bias field was about 5 mG corresponding to a resonance frequency of about 7 kHz. We chose this relatively low magnetic field for several reasons: (i) to ensure that there was no broadening of the resonance due to magnetic-field gradients, (ii) to ensure that fluctuations of the bias magnetic field were much smaller than the width of the

resonance, and (iii) to reduce the requirements on the bandwidth of our photodiode amplifiers. In some measurements, we found a similar sensitivity in bias fields corresponding to 35-kHz resonance frequency. Further work will be needed to understand the limitations of the system at higher bias fields where the noise in the bias field may be comparable to the resonance width or where the nonlinear Zeeman effect becomes significant (studied in a similar context in Ref. [5]). Detection at the photon shot-noise limit for higher frequencies also needs to be demonstrated.

VII. CONCLUSION

In conclusion, we have demonstrated an atomic magnetometric technique for the measurement of small rf magnetic fields based on a ground-state Zeeman resonance and detection of nonlinear magneto-optical rotation in an alkali-metal vapor. We have achieved a sensitivity of about 100 pG/$\sqrt{\text{Hz}}$ (rms) at 7 kHz with a bandwidth of 50–100 Hz based on experimentally measured signal-to-noise ratio in a 3.5-cm-diameter cell. We confirmed experimentally that it is possible to analyze the polarization of the light incident on the balanced polarimeter within 20% the photon shot-noise limit at light powers where the magnetometer achieved the highest sensitivity. The current version of the magnetometer was limited in part because we were not able to collect all of the light that passed through the cell. Assuming better collection and detection of polarization rotation at the photon shot-noise limit, we project a sensitivity as low as 25 pG/$\sqrt{\text{Hz}}$ (rms). The magnetometer operates near room temperature, making it particularly attractive for applications in NMR. One possible such application is the measurement of a scalar, electron-mediated nuclear spin-spin coupling which can yield valuable information on molecular structure.

ACKNOWLEDGMENTS

The authors thank J. Higbie, A. O. Sushkov, and I. M. Savukov for useful comments and discussions. This work was supported by an ONR MURI program and KBN Grant No. 1 P03B 102 30.

[1] A. N. Garroway *et al.*, IEEE Trans. Geosci. Remote Sens. **39**, 1108 (2001).
[2] R. Bradley *et al.*, Rev. Mod. Phys. **75**, 777 (2003).
[3] E. B. Alexandrov, M. V. Balabas, A. S. Pasgalev, A. K. Vershovskii, and N. N. Yakobson, Laser Phys. **6**, 244 (1996).
[4] D. Budker, D. F. Kimball, S. M. Rochester, V. V. Yashchuk, and M. Zolotorev, Phys. Rev. A **62**, 043403 (2000).
[5] V. M. Acosta *et al.*, Phys. Rev. A **73**, 053404 (2006).
[6] I. K. Kominis, T. W. Kornack, J. C. Allred, and M. V. Romalis, Nature (London) **422**, 596 (2003).
[7] I. M. Savukov, S. J. Seltzer, M. V. Romalis, and K. L. Sauer, Phys. Rev. Lett. **95**, 063004 (2005).
[8] P. D. D. Schwindt *et al.*, Appl. Phys. Lett. **85**, 6409 (2004).
[9] R. McDermott *et al.*, Science **295**, 2247 (2002).
[10] S. Appelt, H. Kuhn, F. W. Hasing, and B. Blumich, Nat. Phys. **2**, 105 (2006).
[11] D. Budker, W. Gawlik, D. F. Kimball, S. M. Rochester, V. V. Yashchuk, and A. Weiss, Rev. Mod. Phys. **74**, 1153 (2002).
[12] S. Rochester and D. Budker, Am. J. Phys. **69**(4), 450 (2001).
[13] The counter-rotating component can lead to a shift in the resonance frequency (the Bloch-Siegert effect), however, these shifts are negligible in this work.
[14] S. I. Kanorsky, A. Weis, J. Wurster, and T. W. Hänsch, Phys. Rev. A **47**, 1220 (1993).
[15] J. Brossel and F. Bitter, Phys. Rev. **86**, 308 (1952).
[16] D. Budker, D. F. Kimball, S. M. Rochester, and V. V. Yashchuk, Phys. Rev. Lett. **85**, 2088 (2000).
[17] V. V. Yashchuk *et al.*, Phys. Rev. Lett. **90**, 253001 (2003).
[18] S. Pustelny, D. F. Jackson Kimball, S. M. Rochester, V. V. Yashchuk, W. Gawlik, and D. Budker, Phys. Rev. A **73**, 023817 (2006).
[19] H. G. Robinson, E. S. Ensberg, and H. G. Dehmelt, Bull. Am. Phys. Soc. **3**, 9 (1958).
[20] M. A. Bouchiat and J. Brossel, Phys. Rev. **147**, 41 (1966); M. A. Bouchiat, Ph.D. thesis, University of Paris, 1964.
[21] D. Budker, V. Yashchuk, and M. Zolotorev, Phys. Rev. Lett. **81**, 5788 (1998).
[22] V. Yashchuk, D. Budker, and M. Zolotorev, in *Trapped Charged Particles and Fundamental Physics*, edited by D. H. E. Dubin and D. Schneider (American Institute of Physics, Melville, NY, 1999), pp. 177–181.
[23] S. Pustelny, D. F. Jackson Kimball, S. M. Rochester, V. V. Yashchuk, and D. Budker, Phys. Rev. A **74**, 063406 (2006).
[24] In calculating the photon shot-noise limit, a bandwith of 1 Hz corresponds to a measurement time of 0.5 s.
[25] D. Budker, D. F. Kimball, V. V. Yashchuk, and M. Zolotorev, Phys. Rev. A **65**, 055403 (2002).
[26] For NMOR in the Faraday geometry (see, for example, Ref. [21]), the relaxation rate is $\gamma_{rel}=g\mu_B\Delta B$ where ΔB represents *twice* the distance from the center of the resonance to the extrema of the optical rotation. In the present work, $\Delta\nu$ represents the distance from the center of the resonance to the extrema of the optical rotation. This fact can be verified with a simple treatment of NMOR along the lines of Ref. [14]. The reason for this difference is that the angle between the aligned state and the initial light polarization vector is always small in this work, in contrast to NMOR in the Faraday geometry. This difference in the relationship between the width and relaxation rate can also be illustrated by noting that NMOR in the Faraday geometry involves coherences with $|\Delta M_F|=2$, whereas the coherences involved in the present geometry have $|\Delta M_F|=1$.
[27] M. T. Graf, D. F. Kimball, S. M. Rochester, K. Kerner, C. Wong, D. Budker, E. B. Alexandrov, M. V. Balabas, and V. V. Yashchuk, Phys. Rev. A **72**, 023401 (2005).
[28] D. Budker, L. Hollberg, D. F. Kimball, J. Kitching, S. Pustelny, and V. V. Yashchuk, Phys. Rev. A **71**, 012903 (2005).
[29] E. B. Aleksandrov, M. V. Balabas, A. K. Vershovskii, A. I. Okunevich, and N. N. Yakobson, Opt. Spectrosc. **87**, 329 (1999); **93**, 488(E) (2002).
[30] M. Auzinsh *et al.*, Phys. Rev. Lett. **93**, 173002 (2004).